Current Research in Parasitology & Vector-Borne Diseases 7 (2025) 100251

Contents lists available at ScienceDirect

Current Research in Parasitology & Vector-Borne Diseases

journal homepage: www.sciencedirect.com/journal/current-research-in-parasitology-and-vector-borne-diseases

Transcriptome analysis of *Aedes aegypti* midgut and salivary gland post-Zika virus infection

Chunling Zhu [a,b], Yuting Jiang [a], Qianghui Zhang [a], Jian Gao [a], Chaojie Li [a], Chunxiao Li [a], Yande Dong [a], Dan Xing [a], Hengduan Zhang [a], Teng Zhao [a], Xiaoxia Guo [a,*], Tongyan Zhao [a,**]

[a] *Department of Vector Biology and Control, State Key Laboratory of Pathogen and Biosecurity, Beijing Key Laboratory of Vector Borne and Natural Focus Infectious Diseases, Institute of Microbiology and Epidemiology, Beijing Key Laboratory, Beijing, 100071, China*

[b] *Department of Clinical Laboratory, Guangxi International Zhuang Medicine Hospital Affiliated to Guangxi University of Chinese Medicine, Nanning, 530201, Guangxi, China*

ARTICLE INFO

Keywords:
Zika virus
Aedes aegypti
Vector-pathogen interactions
Transcriptome analysis
miRNA-mRNA network

ABSTRACT

This study aimed to investigate the transcriptomic changes in the midgut and salivary glands of *Aedes aegypti* mosquitoes infected with Zika virus (ZIKV), in order to explore the molecular mechanisms underlying the interaction between the virus and the mosquito vector. *Aedes aegypti* from Jiegao (JG) and Mengding (MD) in China were experimentally infected with ZIKV, and the midgut and salivary gland tissues were collected at 2-, 4- and 6 days post-infection (dpi). High-throughput sequencing was performed to analyze the transcriptomic changes between ZIKV-infected and non-infected *Ae. aegypti* midgut and salivary gland tissues. Bioinformatics tools were employed for further analysis of the transcriptomic data. The expression levels of 8 significantly differentially expressed genes (DEGs) were validated using RT-qPCR. A conjoint analysis of small RNA-seq and mRNA-seq was performed to screen interactional miRNA-mRNA pairs during ZIKV infection. Using the Search Tool for the Retrieval of Interacting Genes, we constructed a protein-protein interaction network of genes and subsequently identified hub genes. The most significant transcriptional changes in *Ae. aegypti* occurred at 2 dpi. On 2, 4 and 6 dpi, 11 genes showed significant changes in both the midgut and salivary glands of the same mosquito strain, while 25 genes exhibited significant changes in the same tissue between the JG and MD strains. The expression tendencies of 8 DEGs obtained by RNA-Seq were similar to those detected by RT-qPCR. Furthermore, we individually identified 10 hub genes in the midgut and salivary glands. Based on previous miRNA research, we discovered the involvement of 9 miRNAs in the regulation of these hub genes. Our findings demonstrate that *Ae. aegypti* exhibit distinct transcriptomic changes in response to ZIKV infection. The identification of the hub genes and their regulatory miRNAs provides valuable insights into the molecular mechanisms underlying ZIKV infection in mosquitoes. This study contributes to a better understanding of the pathogen-vector interactions and may aid in the development of targeted strategies for ZIKV control.

1. Introduction

Zika virus (ZIKV), a member of the family *Flaviviridae*, genus *Flavivirus*, is transmitted by *Aedes* spp. mosquitoes. It was first discovered in 1947 in a rhesus sentinel monkey confined in the Zika forest of Uganda, near Lake Victoria. Subsequently, it was isolated from *Aedes africanus* mosquitoes in the same forest in 1948 (Dick et al., 1952). ZIKV infection in humans was reported during studies in Nigeria in the early 1950's (Macnamara, 1954). The initial ZIKV outbreak occurred in 2007 on Yap Island in Micronesia (Lessler et al., 2016), followed by subsequent outbreaks in Africa, Asia, the Americas, and the Pacific islands. As of December 2021, ZIKV transmission through local mosquitoes has been documented in 89 countries and territories (WHO, 2022). ZIKV infection in humans manifests as high fever, cutaneous rash, joint discomfort, conjunctivitis, headaches, and muscle aches. However, it can also lead to severe and occasionally fatal conditions such as Guillain-Barré syndrome and neonatal microcephaly (Araújo et al., 2016; Brady et al., 2019; Leonhard et al., 2020), posing a significant public health threat.

* Corresponding author.
** Corresponding author.
E-mail addresses: guoxx99@163.com (X. Guo), tongyanzhao@126.com (T. Zhao).

https://doi.org/10.1016/j.crpvbd.2025.100251
Received 23 August 2024; Received in revised form 23 February 2025; Accepted 24 February 2025
Available online 26 February 2025

Currently, specific antiviral drugs or vaccines against ZIKV infection are not available, making vector control the primary method to mitigate transmission risk. Yet, the efficacy of current vector control methods is limited. Therefore, there is an urgent need for innovative strategies to control the spread of arboviruses.

ZIKV primarily infects humans through the bites of *Aedes* spp. mosquitoes, particularly *Aedes aegypti*. The virus must successfully traverse the midgut tissue, which is considered the initial obstacle to infection, before disseminating to other tissues and eventually reaching the salivary glands (Zimler et al., 2021; Jia et al., 2023). In the salivary glands, ZIKV is released into salivary ducts and transmitted to human hosts during subsequent blood-feeding events (Zimler et al., 2021). In mosquitoes, several innate immune pathways, such as Toll, immune deficiency (IMD), and Janus kinase/signal transducer and activator of transcription (JAK/STAT) signaling pathways, have been demonstrated to inhibit viral replication under specific conditions. There is also the RNA interference (RNAi) pathway, which is widely recognized as the key mechanism by which mosquitoes resist viral infections. Studies have shown that after mosquito-borne viruses infect mosquitoes, the activation of the mosquito immune system can limit their replication both inside and outside the mosquito body. However, mosquito-borne viruses are not completely eliminated, which may be related to immune escape (Prince et al., 2023). The interaction between viruses and the mosquito immune system is relatively complex and has not yet been fully elucidated. Multiple studies have found that the transcriptome expression profiles of mosquitoes undergo significant changes after mosquito-borne virus infection. For example, a study found that the transcriptome expression profiles of *Ae. aegypti* changed significantly at different time points after ZIKV infection, and most of the altered genes were involved in metabolic processes, cellular processes, and protein degradation (Etebari et al., 2017). Another study analyzed the gene expression changes in *Ae. aegypti* after ZIKV infection through transcriptome sequencing and found that a calreticulin-like (CRT) gene was significantly upregulated during the infection process. However, when qPCR was used to verify the CRT expression between infected and uninfected female mosquitoes, no significant difference was found. This may be because CRT expression varies among individuals, changes over time, and is affected by viral load. Further research is needed to explore its role in the interaction between the virus and mosquitoes (Almeida et al., 2023). Additionally, a study assessed the vector competence of *Aedes albopictus* from Jinghong and Guangzhou, China, for ZIKV and sequenced the transcripts of midgut and salivary gland tissues 10 days after infection. It was found that *Ae. albopictus* from both locations were susceptible to ZIKV, but the Guangzhou strain had stronger vector competence. Moreover, there were significant differences in the categories and functions of differentially expressed genes responding to ZIKV infection in different tissues and strains, indicating that the different vector competences of *Ae. albopictus* for ZIKV may be related to different strains and tissues (Jia et al., 2023). These studies indicate that the interaction between ZIKV and mosquitoes is complex and diverse, involving multiple molecular mechanisms. Therefore, more research is needed to identify the host factors involved in viral replication or antiviral responses of mosquito hosts.

A previous study has demonstrated that Jiegao (JG) and Mengding (MD) strains of *Ae. aegypti* display strong vector competence for ZIKV. Additionally, changes in microRNA (miRNA) profiles were observed in the midgut and salivary gland of these *Ae. aegypti* strains at three different time points following ZIKV infection (Zhu et al., 2021). However, the study by Zhu et al. (2021) primarily focused on the miRNA profiles and did not provide a comprehensive analysis of the transcriptomic changes in these tissues. Here, we performed high-throughput sequencing of the transcriptome in the midgut and salivary gland of ZIKV-infected *Ae. aegypti* at the same time points and also conducted a conjoint analysis of small RNA-seq and mRNA-seq to identify interactional miRNA-mRNA pairs during ZIKV infection. Our objective was to investigate the molecular interactions between the mosquito host and the virus, which may contribute to the development of novel strategies for preventing insect-borne diseases.

2. Materials and methods

2.1. Virus strain

The virus strain used in this study was ZIKV SZ01, obtained from the Microbial Culture Collection Center of the Beijing Institute of Microbiology and Epidemiology. This virus was initially discovered in a patient returning from Samoa to China in 2016 (GenBank: KU866423) (Deng et al., 2016). Before the study, the virus was passaged four times in the *Ae. albopictus* C6/36 cell lines.

2.2. Infection of mosquitoes

Two strains of *Ae. aegypti* (JG and MD) were originally collected from Jiegao (23°58′40"N, 97°53′24"E) and Mengding (23°33′00"N, 99°3′33"E), Yunnan Province, China, respectively, in 2018. Both mosquito strains were reared under the same conditions (temperature of 26 ± 1 °C, relative humidity of 75 ± 5%, and a 14:10-h light/dark photoperiod). Adult mosquitoes were provided with a 10% sucrose solution.

Five-day-old nulliparous female *Ae. aegypti* mosquitoes were orally infected with viral blood meals containing a 1:1 mixture of mouse blood and ZIKV SZ01 strain suspension using the Hemotek membrane feeding system (Sihuan, Beijing, China) to keep the virus blood meal at 37 °C. The titer of the viral blood meal was 1.5×10^4 PFU/ml. The non-infected group was fed with blood meals without ZIKV. After 1 h of blood-feeding, fully engorged mosquitoes were transferred to plastic cups and reared under standard conditions.

2.3. Sample preparation for mRNA-seq

The midguts and salivary glands of infected and uninfected mosquitoes were dissected at 2-, 4-, and 6 days post-infection (dpi). A total of 24 groups, each consisting of approximately 100 mosquito samples, were used to create RNA-seq libraries. These tissues were collected in 1.5 ml RNase-free microcentrifuge tubes containing 500 μl TRIzol reagent (Invitrogen, Carlsbad, USA) and stored at −80 °C until subsequent RNA extraction.

2.4. RNA extraction, mRNA library preparation and sequencing

The RNA extraction, library preparation, and sequencing analyses were performed by BGI Company (Shenzhen, China). Total RNA was extracted from each group using TRIzol reagent according to the manufacturer's protocol. The quality and quantity of RNA were assessed using Agilent 2100 (Agilent, Santa Clara, USA). Each RNA sample was split into two sections: one for mRNA library preparation and sequencing, and the other for real-time quantitative PCR (RT-qPCR) analysis. Oligo(dT) magnetic beads were used for the enrichment of mRNAs with a poly(A) tail. After fragmenting the purified mRNA, random N6 primers were employed for reverse transcription, and double-stranded cDNA was synthesized. The synthesized double-stranded DNA was flattened, while the 5′-end was phosphorylated and the 3′-end was added with an A-tail. Following PCR amplification, the PCR product was denatured into single-stranded DNA, which was then cyclized to obtain a single-stranded circular DNA library. The quality of the cDNA was assessed using Agilent 2100 (Agilent). Subsequently, the mRNA libraries were sequenced using Illumina genomic analyzer.

2.5. Bioinformatics

Filtering the original data is crucial to ensure the quality and reliability of the data analysis. We utilized SOAPnuke v1.5.2 (Cock et al., 2010) to eliminate reads containing adapters, undetermined base

information, and low quality. To determine the mapping position of the reads on the reference genome, clean reads were mapped to the reference genome using HISAT2 v2.0.4 (Kim et al., 2015). Bowtie2 (v2.2.5) (Langmead and Salzberg, 2012) was employed to align the clean reads to the reference coding gene set, and then RSEM (v1.2.12) (Li and Dewey, 2011) was used to estimate the gene expression levels. Lastly, the genes were subjected to enrichment analysis based on Gene Ontology (GO; http://amigo.geneontology.org/amigo) and the Kyoto Encyclopedia of Genes and Genomes (KEGG; https://www.genome.jp/kegg/pathway.html).

2.6. Expression profiling of mRNAs in response to ZIKV

An algorithm was employed to analyze the differentially expressed mRNAs between ZIKV-infected and non-infected groups: $p(\chi) = e^{-\lambda}\lambda^{\chi}/\chi!$, where χ is defined as the number of reads from mRNA, and λ is the real number of transcripts of the mRNA. The detailed methodology was described by Audic and Claverie (1997). Significantly differentially expressed genes were determined using the threshold parameters of FDR < 0.001 and $|\log2(FC)| > 1$.

2.7. RT-qPCR analysis of mRNAs

The expression of 8 mRNA transcripts was validated by two-step RT-qPCR using the primers shown in Supplementary Table S1. Reverse transcription (RT) reaction was conducted in a mixture containing 6 μl of RNase-free water, 0.5 μl of RNase inhibitor (50 U/μl), 2 μl RT Primer (50 pM/μl), 2 μl of total RNA, incubated at 65 °C for 5 min, 37 °C for 10 min and centrifuged at high speed (> 5000 *g*) for 5 s. Then, the solution was mixed with 0.5 μl of RNase inhibitor (50 U/μl), 4 μl of 5× Buffer, 2 μl of dNTP (10 mM each), 2 μl of DTT and 1 μl AMV (200 U/μl) and incubated at 40 °C for 1 h, 90 °C for 5–10 min, 4 °C for 5 min and centrifuged at high speed (> 5000 *g*) for 5 s. All RT reagents were purchased from Invitrogen (Carlsbad, CA, USA). The resulting cDNA were used as templates for qPCR reaction, which contains 8 μl of 2× PCR mix (Qiagen, Hilden, Germany), 0.2 μl of each forward and reverse primers, 1 μl of template and 6.6 μl of nuclease-free water. qPCR was performed in an ABI Vii 7 PCR system programmed as follows: 1 cycle at 95 °C for 2 min, 94 °C for 10 s, and 40 cycles at 59 °C for 10 s and 72 °C for 40 s. The analysis of qPCR results was performed using $2^{-\Delta\Delta Ct}$ method (Livak and Schmittgen, 2001). Ribosomal Protein S7 RNA was used to normalize the fold changes in mRNA expression in each sample.

2.8. Correlation analysis of miRNAs and mRNAs

A previous study screened for differentially expressed miRNAs in the JG and MD strains of *Ae. aegypti* infected with ZIKV (Zhu et al., 2021). In the present study, the mRNA corresponding to these differentially expressed miRNA were identified by intersecting with the differentially expressed mRNA in JG and MD strains following ZIKV infection. Candidate target gene pairs were selected based on the regulatory principle of miRNA-mRNA interactions, including significantly downregulated miRNA and upregulated mRNA, as well as significantly upregulated miRNA and downregulated mRNA. The miRNA-mRNA interaction network was constructed using Cytoscape-3.10.0, incorporating the miRNA-mRNA data obtained from the aforementioned selection criteria. The interaction gene retrieval tool (STRING) is an interactive gene database designed to analyze PPI information (Szklarczyk et al., 2019). In STRING, overlapping genes are mapped to generate functional protein-protein interaction networks. Subsequently, Cytoscape-3.10.0 is used for visualization of the PPI network. Additionally, we utilized the cytoHubba plugin to identify hub genes using the Maximum Clique Centrality (MCC) method and performed further analysis on the top 10 hub genes with the highest MCC scores (Chin et al., 2014).

3. Results

3.1. Analysis of Ae. aegypti transcriptome using RNA sequencing (RNA-seq)

The transcriptome of 24 samples from ZIKV-infected and non-infected *Ae. aegypti* mosquitoes was sequenced using the Illumina high-throughput sequencing platform. The samples were collected at 2-, 4-, and 6 days post-infection (dpi). Each library produced approximately 21.62–22.75 Mb of raw reads, and after removing low-quality reads and reads without proper mapping, approximately 21.07–21.89 Mb of clean reads were obtained. The mapping results demonstrated that about 87.8–90.89% of the reads per sample were successfully mapped to the genome (Supplementary Table S2).

3.2. Analysis of mRNA expression differences

The analysis of mRNA expression profiles in ZIKV-infected *Ae. aegypti* midgut tissue revealed a total of 1359 and 4496 differentially expressed genes ($|\log2\ FC| > 1$) in the JG strain and MD strain, respectively, at the three time points compared to non-infected controls. The most pronounced changes among the three time points were observed at 4 dpi, with 822 differentially expressed genes in the JG strain, and at 2 dpi, with 3724 differentially expressed genes in the MD strain.

Additionally, the salivary gland tissue of ZIKV-infected *Ae. aegypti* showed 1292 and 8620 differentially expressed genes in the JG strain and MD strain, respectively, compared to their respective control groups. The highest number of gene alterations occurred at 2 dpi for both *Ae. aegypti* strains (Fig. 1). The differences in the number and timing of DEGs in the transcriptome of *Ae. aegypti* JG and MD strains after ZIKV infection may be closely related to the genetic background of the mosquitoes.

3.3. Overlapping genes in the midgut and salivary glands of Ae. aegypti at three time points following ZIKV infection

Comparing the transcriptome profiles of ZIKV-infected *Ae. aegypti*, we identified 51 overlapping genes (JG strain) and 55 overlapping genes (MD strain) in the midgut tissue, and 68 overlapping genes (JG strain) and 118 overlapping genes (MD strain) in the salivary gland tissue across the three time points (Fig. 2). On 2, 4 and 6 dpi, 3 genes from JG strains and 8 genes from MD strains showed significant changes in both the midgut and salivary gland of the same mosquito strain (Table 1). Furthermore, we found that 9 genes in the midgut tissue and 16 genes in the salivary gland tissue were consistently altered in both JG and MD strains following ZIKV infection (Table 2). Among these genes, 7 were upregulated and one gene was downregulated in the midgut tissue, displaying the same tendency in both *Ae. aegypti* strains. Interestingly, one gene (AAEL013535) was upregulated only at 2 dpi in the midgut of the JG strain and exhibited opposite regulation in the MD strain and other time points in the JG strain. However, in the salivary gland tissue, only one gene (5576721) showed consistent regulation by both JG and MD strains across the three time points, while the remaining 15 genes exhibited opposite regulation at different time points.

3.4. RT-qPCR validation of differentially expressed genes

To validate the results of RNA-Seq data, we determined the expression of 8 genes in the midgut and salivary gland tissue (AAEL004805, AAEL005951, AAEL009596, AAEL012644, AAEL013535, AAEL006485, AAEL009524, AAEL005849), with reverse transcription-quantitative PCR (RT-qPCR) assays on 2, 4 and 6 dpi for both the JG and MD strains (Fig. 3). The expression tendencies of these genes obtained by RNA-Seq were similar to those detected by RT-qPCR, indicating that results from RNA-Seq data were reliable.

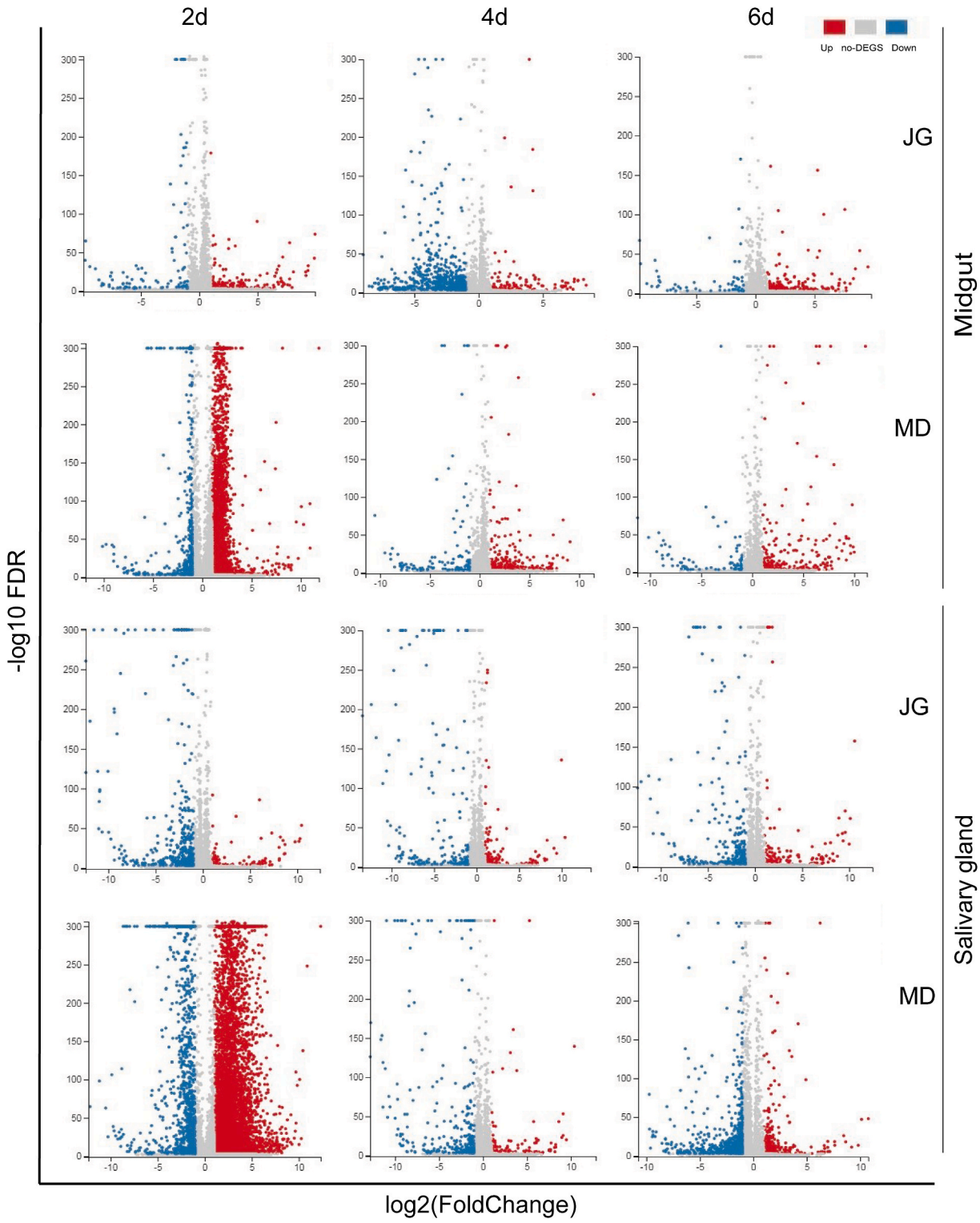

Fig. 1. Volcano plots of differentially expressed genes. Gene expression levels in the midgut or salivary gland of the two *Ae. aegypti* strains (JG and MD) infected with ZIKV at the indicated time points are compared with those of the control group. The genes with $|\log2\ FC| > 1$ and FDR <0.001 were considered to be significantly changed. Red and green plots indicate significantly upregulated (Up) and downregulated (Down) expression, respectively. Grey plots (non-DEGs) indicate no significant difference between infected and control libraries.

3.5. Conjoint analysis of small RNA-Seq and mRNA-Seq

A negative correlation analysis was conducted on the differentially expressed miRNAs and mRNAs in JG and MD strains of *Ae. aegypti* after ZIKV infection. In the midgut, a total of 8 miRNA-mRNA pairs (2 pairs at 2 dpi, 5 pairs at 4 dpi, and 1 pair at 6 dpi) were identified in the JG strain, while 240 miRNA-mRNA pairs (226 pairs at 2 dpi, 11 pairs at 4 dpi, and 3 pairs at 6 dpi) were identified in the MD strain. Furthermore, in the salivary glands, 19 miRNA-mRNA pairs (11 pairs at 2 dpi, 2 pairs at 4 dpi, and 6 pairs at 6 dpi) were identified in the JG strain, while 334 miRNA-mRNA pairs (180 pairs at 2 dpi, 20 pairs at 4 dpi, and 134 pairs at 6 dpi) were identified in the MD strain (Supplementary Table S3). A

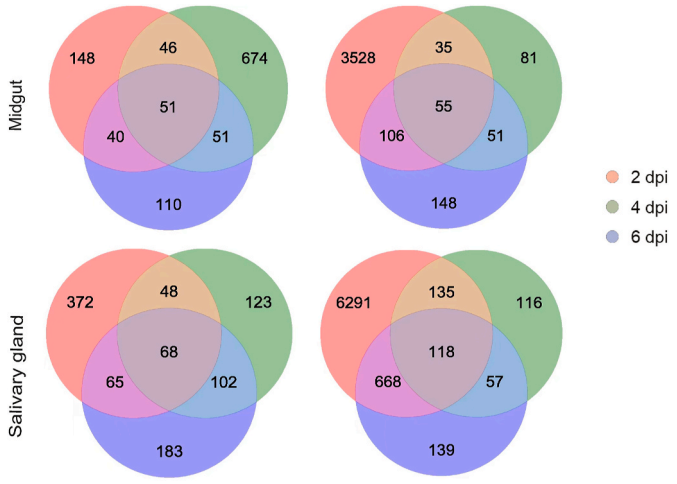

Fig. 2. Venn diagram representing the number of differentially expressed genes of the two *Ae. aegypti* strains (JG and MD) at three different time points post-ZIKV infection.

network association graph for these miRNA-mRNA pairs was constructed (Fig. 4). Using the MCC algorithm in the cytoHubba plugin of Cytoscape-3.10.0, the top 10 hub genes in the midgut and salivary glands were selected (Fig. 4A–C). To further investigate the expression and regulatory relationships among the hub genes, a network association graph between the hub genes and miRNAs was constructed. In the network association graph, 10 hub genes in the midgut were regulated by novel_mir65 (Fig. 4B), while in the salivary glands, AAEL000010 and AAEL002639 were regulated by aae-miR-276-3p; AAEL010168 and AAEL009078 were regulated by novel_mir43; AAEL013533 was regulated by aae-miR-263b-5p; AAEL002047 was regulated by aae-miR-275-3p; AAEL000138 was regulated by aae-miR-2b; AAEL007771-PB was regulated by novel_mir15; AAEL014889 was regulated by novel_mir17; and AAEL008329 was regulated by novel_mir56 (Fig. 4D).

3.6. GO/KEGG pathway

To further investigate the biological functions of the hub genes among the three time points in two *Ae. aegypti* strains after ZIKV infection, GO terms were used to classify the functions of these genes (Fig. 5). In the functional enrichment analysis of hub genes in midgut tissue, the annotation of biological processes revealed that most genes were associated with biological regulation, regulation of cellular process, and regulation of biological process. The cell component annotation showed that most genes were related to nucleoplasm. The molecular function annotation indicated that virus-infected cells frequently displayed functional alterations related to catalytic activity and transferase activity (Fig. 5A). In contrast, the functional enrichment of hub genes in salivary glands showed differences compared to the midgut. The annotation of biological processes revealed that most genes were associated with nitrogen compound metabolic process, cellular nitrogen compound metabolic process, and organonitrogen compound metabolic process. The cell component annotation showed that most genes were related to intracellular organelles, cytoplasm, and cytoplasmic part. The molecular function annotation indicated that virus-infected cells frequently displayed functional alterations related to a structural constituent of the ribosome and structural molecule activity (Fig. 5B).

According to the KEGG pathway analyses, the hub genes in the midgut tissue are involved in the response to the Wnt signaling pathway, TGF-beta signaling pathway, FoxO signaling pathway, MAPK signaling pathway - fly, and Dorso-ventral axis formation (Fig. 5C). On the other hand, the hub genes in the salivary glands are predominantly enriched in two pathways, namely Ribosome and Oxidative phosphorylation (Fig. 5D).

4. Discussion

ZIKV is a rapidly emerging infectious disease that poses a significant threat to public health. Previous studies have focused on understanding the molecular interactions between ZIKV and *Ae. aegypti* through changes in small RNA and transcriptome expression (Etebari et al., 2017; Zhu et al., 2021; Almeida et al., 2023). However, the tissue-specific responses during the infection process remain poorly understood. Upon ingestion of an infectious blood meal, the midgut of the mosquito acts as the primary barrier for arbovirus replication, while the salivary glands plays a crucial role in efficient arbovirus transmission (Cui et al., 2019; Sanchez-Vargas et al., 2021). In our study, we aimed to investigate the virus-vector interactions occurring in the midgut and salivary gland tissues upon ZIKV infection at three time points. Our results demonstrate that the most significant changes in transcript levels within the midgut and salivary gland tissues of ZIKV-infected *Ae. aegypti* mosquitoes occur predominantly at 2 dpi compared to other time points. This suggests that the modulation of gene expression in the midgut and salivary gland tissues is most pronounced early in the infection process. However, in a previous transcriptomic study that examined the impact of ZIKV on the overall transcriptome of *Ae. aegypti* mosquitoes using RNA-Seq, the highest number of altered genes was observed at 7 dpi, while the numbers of altered genes at 2 dpi and 14 dpi were lower (Franz et al., 2015). This indicates that the regulation of viral infection is tissue-specific and dependent on mosquito and viral genotypes.

In the study conducted by Londono-Renteria et al. (2015) differentially expressed genes were observed in *Ae. aegypti* following infection with yellow fever virus (YFV), dengue virus (DENV), and West Nile virus (WNV). Additionally, in another study on ZIKV infection in *Ae. aegypti*, 5

Table 1
DEGs in the midgut and salivary gland tissues of the same *Ae. aegypti* strain at three time points after ZIKV infection.

Gene ID		Gene description	Strain	log2 FC					
				Midgut			Salivary gland		
				2 dpi	4 dpi	6 dpi	2 dpi	4 dpi	6 dpi
5569630	AAEL007780	Uncharacterized LOC5569630	JG	1.18	2.47	1.99	−5.17	−5.30	−4.49
5577338	AAEL000442	Maternal effect protein oskar	JG	6.84	−4.21	3.29	−3.25	−1.98	2.10
5579856	AAEL005849	Synaptic vesicle glycoprotein 2C	JG	2.54	4.22	5.78	−1.42	−1.58	−2.63
5569242	AAEL005849	Synaptic vesicle glycoprotein 2A	MD	1.92	4.17	6.98	−2.42	3.21	2.95
5569528	AAEL007703	Uncharacterized LOC5569528	MD	1.15	2.60	6.27	−5.02	3.46	4.20
5571793	AAEL009309	Protein Peter Pan	MD	−7.02	7.29	9.20	6.81	−1.81	8.45
5576617	AAEL012644	Uncharacterized LOC5576617	MD	2.62	2.57	6.49	−5.64	3.85	3.60
5576619	AAEL012646	Uncharacterized LOC5576619	MD	2.75	3.40	4.98	−4.57	5.87	2.68
5576969	–	UDP-glucuronosyltransferase 2B18	MD	2.08	2.81	4.42	1.50	5.29	1.25
23687754	AAEL017334	Flocculation protein FLO11	MD	2.37	2.74	6.60	−3.51	3.13	6.26
110673979	AAEL001085	Mitochondrial intermembrane space import and assembly protein 40	MD	−1.01	−8.01	−2.07	−8.20	9.12	−1.60

Abbreviations: JG, Jiegao; MD, Mengding; dpi, days post-infection.

Table 2
DEGs in the same tissues of two *Ae. aegypti* strains (JG and MD) at three time points after ZIKV infection.

Gene ID		Gene description	Tissue	log2 FC					
				JG			MD		
				2 dpi	4 dpi	6 dpi	2 dpi	4 dpi	6 dpi
5564054	AAEL004048	UNC93-like protein	M	1.81	4.29	2.44	1.75	2.73	8.08
5565499	AAEL004805	Sodium/potassium/calcium exchanger 4	M	1.70	1.64	3.31	1.69	2.55	6.31
5566438	AAEL005385	Uncharacterized LOC5566438	M	2.08	4.41	4.05	3.71	2.78	5.49
5569242	AAEL007489	Synaptic vesicle glycoprotein 2A	M	1.92	4.69	4.01	1.92	4.17	6.98
5571480	AAEL010921	Solute carrier organic anion transporter family member 2A1	M	1.90	3.70	3.39	3.93	3.60	7.27
5572188	AAEL009596	Sterol O-acyltransferase 1	M	−2.31	−1.76	−1.13	−1.03	−2.10	−1.33
5576617	AAEL012644	Uncharacterized LOC5576617	M	2.05	4.23	2.59	2.62	2.57	6.49
5577500	AAEL003184	Solute carrier family 22 member 21	M	2.18	3.71	3.26	2.64	3.04	6.17
5578159	AAEL013535	Arrestin homolog	M	1.62	−3.83	−2.98	−1.61	−2.68	−3.35
5566809	AAEL005656	Myosin heavy chain, muscle	SG	−2.02	−1.33	−2.15	2.40	−2.31	−2.17
5567956	AAEL006417	37 kDa salivary gland allergen Aed a 2-like	SG	−1.37	−5.02	−3.67	3.32	−9.32	−7.98
5568044	AAEL006485	Probable uridine nucleosidase 1	SG	−1.66	−5.04	−4.53	2.74	−8.03	−2.59
5569630	AAEL007780	Uncharacterized LOC5569630	SG	−5.17	−5.30	−4.49	−3.02	−1.37	3.47
5569903	AAEL007986	Uncharacterized LOC5569903	SG	−10.60	−8.65	−6.06	2.58	−8.82	−8.13
5570845	AAEL008619	Kallikrein 1-related peptidase b3	SG	−1.84	−5.61	−3.84	2.58	−8.42	−6.81
5571443	AAEL009081	Uncharacterized LOC5571443	SG	−9.21	−8.98	−6.52	1.70	−9.70	−6.82
5572111	AAEL000392	Probable maltase	SG	−5.14	−6.19	−5.39	3.29	−5.85	−1.19
5572722	AAEL009993	Uncharacterized LOC5572722	SG	−1.06	−5.02	−4.23	5.78	−7.61	−4.00
5576721	–	COX assembly mitochondrial protein 2 homolog	SG	8.10	7.13	7.92	1.76	1.48	7.15
5577338	AAEL000442	Maternal effect protein oskar	SG	−3.25	−1.98	2.10	4.46	−3.07	−7.00
5579856	AAEL005849	Synaptic vesicle glycoprotein 2C	SG	−1.42	−1.58	−2.63	−2.76	2.23	2.44
23687754	AAEL017334	Flocculation protein FLO11	SG	−1.75	2.32	−3.82	−3.51	3.13	6.26
110675441	–	Biofilm and cell wall regulator 1-like	SG	−9.23	−8.81	−6.29	3.05	−10.04	−8.40
110680819	–	Uncharacterized protein C12orf73 homolog	SG	10.19	10.40	9.99	−5.31	1.56	10.76
110681458	–	Transcription factor TFIIIB component B″ homolog	SG	−6.23	−4.91	−6.29	6.88	2.67	6.97

Abbreviations: M, midgut; SG, salivary gland; dpi, days post-infection.

of 20 genes also displayed significant differential expression (Etebari et al., 2017). In our study, we also observed two of these genes differentially expressed significantly, AAEL000379 (cysteine-rich venom protein 379, CRVP379) and AAEL013122. CRVP379 exhibited a downregulation of 4.24-fold in the midgut tissue of the JG strain compared to the control group, while in the midgut tissue of the MD strain, it showed an upregulation of 9.06-fold. In the salivary gland tissue, CRVP379 displayed a 3.32-fold upregulation in the JG strain, while no significant differential expression was observed in the MD strain. AAEL013122, on the other hand, showed significant downregulation of 4.54-fold, specifically in the salivary gland tissue of the MD strain. Although both studies focused on Zika virus (ZIKV) infections in *Ae. aegypti*, Etebari et al. (2017) utilized whole mosquitoes whereas our study specifically examined the midgut and salivary gland tissues. This suggests potential variations in gene expression regulation in different geographical strains and mosquito organs. Furthermore, Londono-Renteria et al. (2015) demonstrated that silencing the gene CRVP379 led to a reduction in dengue virus (DENV) replication. Another study demonstrated that *Ae. aegypti* with the CRVP379 gene knocked out, when infected with DENV, did not exhibit significant changes in midgut DENV replication; however, these mosquitoes showed a significant decrease in egg-laying quantity and a marked reduction in egg hatching rates (Tikhe et al., 2022). The differences in these two studies may potentially be attributed to different factors such as experimental methods and experimental conditions. Nevertheless, these studies have demonstrated that CRVP379 exhibits complex and multifaceted functions. It not only affects the replication of DENV within *Ae. aegypti* but also significantly impacts its reproductive capacity. However, there are currently no reports on the influence of CRVP379 on the replication of ZIKA in *Ae. aegypti*. Therefore, further research is needed to thoroughly explore the mechanism by which CRVP379 acts in the replication of ZIKA. In addition, the role of AAEL013122 in virus-mosquito interactions remains unclear at present, and further experiments are needed for its exploration.

Our results revealed significant variations in DEGs between the two tissue types of the same mosquito strain and within the same tissue type of two different mosquito strains. A total of 36 overlapping genes were identified, including sodium/potassium/calcium exchange 4, synaptic vesicle glycoprotein 2A, arrestin homolog, myosin heavy chain, muscle, biofilm and cell wall regulator 1-like, and transcription factor TFIIIB component B homolog, among others. Previous studies have shown that during the invasion of the midgut of *Anopheles albimanus* by *Plasmodium vivax*, myosin (AALB007909) acts as a key target, providing the power for the movement and entry of the malaria parasite into the mosquito midgut epithelial cells, enabling the parasite to effectively penetrate the cellular barrier and complete the invasion process (Lecona-Valera et al., 2016). This suggests that myosin may be an important protein for pathogen infection of mosquitoes. However, there are currently no studies reporting its role in the viral infection of mosquitoes. Our study demonstrated significant downregulation of arrestin homolog and myosin in the midgut tissue of MD strains at three distinct time points following ZIKV infection. Therefore, future research can explore the potential role of myosin in ZIKA-infected mosquitoes, which will help us gain a more comprehensive understanding of the interaction mechanisms between ZIKA and mosquito hosts. Furthermore, other overlapping genes also displayed significant changes, suggesting their important regulatory role in ZIKV infection in mosquitoes.

Several studies have demonstrated the important role of miRNAs in virus infection by regulating the expression of target genes. For instance, aae-miR-989 is involved in the replication of dengue virus (DENV) in *Ae. aegypti* by negatively regulating the expression of the AaATL gene (Hussain et al., 2022). Building upon previous research (Zhu et al., 2021), we constructed a miRNA-mRNA regulatory network, in which 10 hub genes in the midgut were found to be regulated by novel_mir65. Furthermore, novel_mir65 was downregulated in our experiments, whereas the expression levels of the 10 hub genes were upregulated. This suggests that novel_mir65 may regulate the interaction between ZIKV and *Ae. aegypti* by targeting these genes and influencing relevant pathways. Novel_mir65 is a newly discovered miRNA in this study, which has not yet been identified or named. Therefore, further investigations are needed to explore its specific regulatory mechanisms. In contrast to the midgut, the 10 hub genes in the salivary glands are

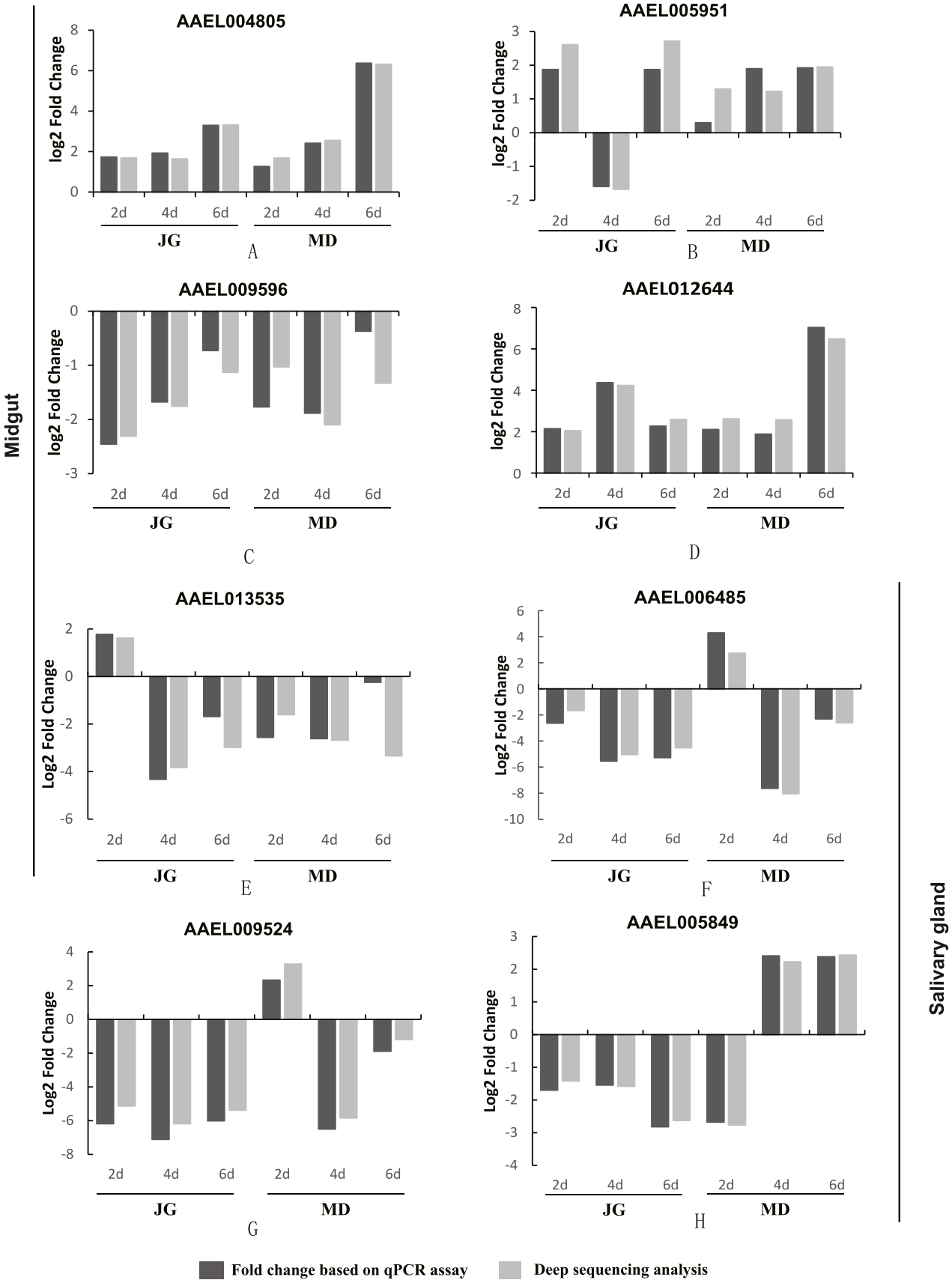

Fig. 3. RT-qPCR verification of differentially expressed genes from RNA-Seq. Gene expression in the midgut (**A**–**E**) and salivary gland (**F**–**H**) of the two *Ae. aegypti* strains (JG and MD) infected with ZIKV relative to the uninfected group at the indicated time-point. For the RT-qPCR assay, fold changes are averages of three technical replicates.

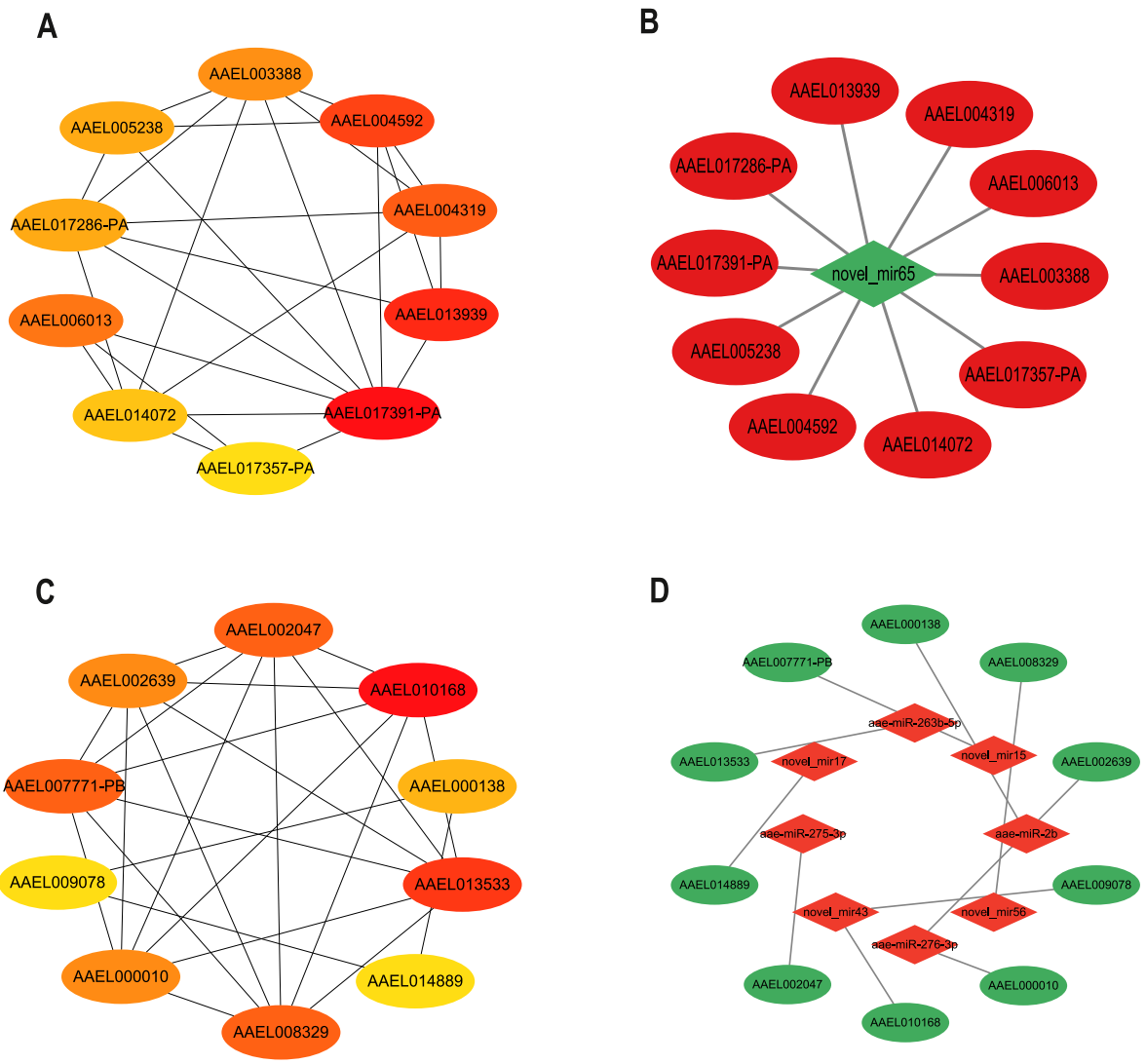

Fig. 4. Conjoint analysis of miRNA and RNA-seq in *Ae. aegypti* infected with ZIKV. **A**, **C** Hub genes in the midgut (**A**) and salivary gland (**C**) of the two *Ae. aegypti* strains (JG and MD) infected with ZIKV. **B**, **D** miRNA-hub genes in the midgut (**B**) and salivary gland (**D**) of the two *Ae. aegypti* strains infected with ZIKV. Red and green plots indicate significantly upregulated and downregulated expression, respectively (panels **B** and **D**). The shades of red, orange, and yellow, from dark to light, represent the MCC scores of the hub genes, from high to low (panels **A** and **C**).

regulated by 8 different miRNAs, including 4 novel miRNAs identified in the present study.

This study conducted a conjoint analysis of sRNA-seq and mRNA-seq in the midgut and salivary glands of *Ae. aegypti* infected with ZIKV and identified 10 key hub genes (AAEL004592, AAEL005238, AAEL017391-PA, AAEL017286-PA, AAEL013939, AAEL004319, AAEL014072, AAEL006013, AAEL003388, AAEL017357-PA). Gene ontology (GO) enrichment analysis revealed that these hub genes in the midgut are mainly involved in biological regulation, transferase activity, catalytic activity, and other functions. The enriched pathways primarily include the Wnt signaling pathway, TGF-beta signaling pathway, FoxO signaling pathway, and MAPK signaling pathway - fly. Previous studies have shown that tyrosine-protein kinase Src64B (AAEL005238) can restrict the replication of White Spot Syndrome Virus (WSSV) in shrimp by regulating cell apoptosis (Wei et al., 2019). Glycogen synthase kinase-3 beta (AAEL005238) acts as a drug target to activate the Wnt/β-catenin pathway, leading to the augmentation of the host's immune response and suppression of viral replication (Wang et al., 2023). CREB-binding protein (AAEL017391-PA) facilitates viral replication within astrocytes, during ZIKV infection of the mammalian central nervous system (Sun et al., 2020). Histone acetyltransferase Tip60 (AAEL014072) inhibits the replication of influenza A virus by activating the TBK1-IRF3 signaling pathway (Ma et al., 2018). These studies indicate the significant roles of these 4 genes in regulating viral replication, but their functions in mosquitoes remain unknown. Among the 10 hub genes in the salivary glands (AAEL013533, AAEL002047, AAEL000010, AAEL002639, AAEL000138, AAEL007771-PB, AAEL014889, AAEL010168, AAEL009078, AAEL008329), their main functions are related to intracellular organelles, ribosomes, cellular nitrogen compound metabolic processes and so on. The enriched pathways are primarily Ribosome and Oxidative phosphorylation. It has been shown that 40S ribosomal protein S2 (AAEL010168) is significantly upregulated in *Ae. aegypti* infected with dengue fever and Rift Valley fever viruses (Licciardi et al., 2020). However, in the present study, the expression of AAEL010168 was downregulated in the salivary glands of *Ae. aegypti* infected with ZIKV, indicating its important role in the mosquito-virus interaction, but the specific mechanism remains unclear.

Overall, our study provides a comprehensive analysis of the transcriptomic changes occurring in *Ae. aegypti* upon ZIKV infection. The identification of candidate genes and miRNAs provides new insights into the molecular mechanisms underlying mosquito susceptibility to ZIKV infection and host-pathogen interactions. These results will contribute to

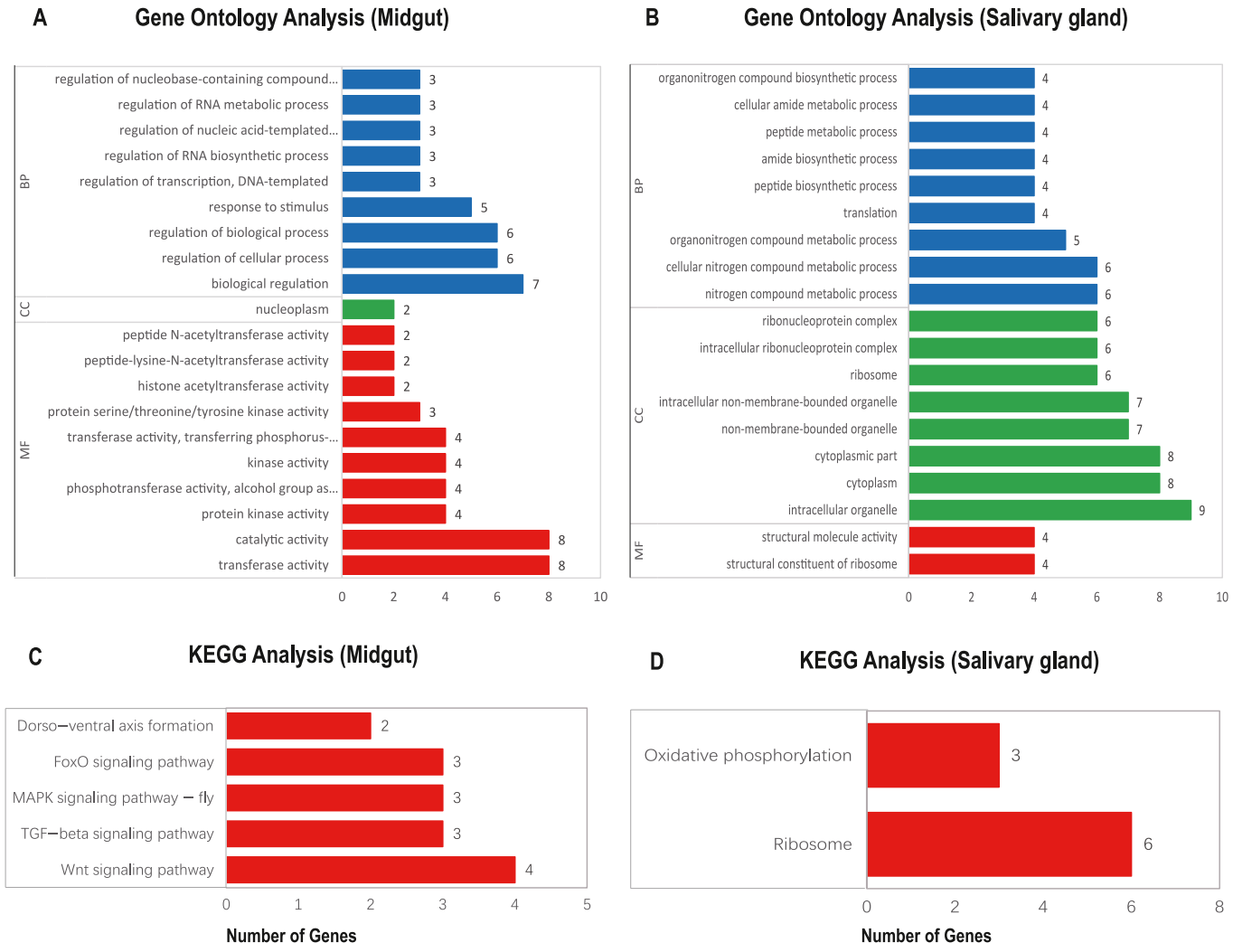

Fig. 5. Gene Ontology (GO) and KEGG analysis on hub genes of the two *Ae. aegypti* strains (JG and MD) infected with ZIKV. **A**, **B** GO analysis in the midgut (**A**) and salivary gland (**B**). **C**, **D** KEGG analysis in the midgut (**C**) and salivary gland (**D**). *Abbreviations*: BP, Biological Process; CC, Cellular Component; MF, Molecular Function.

our understanding of ZIKV transmission and may inform the development of novel vector control strategies. In subsequent studies, we will explore and investigate the roles of these genes in the interaction between mosquitoes and ZIKV.

5. Conclusions

In this study, we investigated the transcriptomic changes in the midgut and salivary glands of *Ae. aegypti* mosquitoes from JG and MD in response to ZIKV infection. Our results demonstrated that both JG and MD strains of *Ae. aegypti* are susceptible to ZIKV, but significant differences in transcriptional profiles were observed between the two strains. The most significant transcriptomic changes occurred at 2 dpi. A total of 11 genes showed significant changes in both the midgut and salivary glands within the same mosquito strain, while 25 genes exhibited significant differences in the same tissue between the JG and MD strains. We identified 8 DEGs whose expression levels were validated by RT-qPCR, and 10 hub genes in the midgut and salivary glands, regulated by 9 miRNAs. These findings provide new insights into the molecular mechanisms underlying ZIKV infection in mosquitoes and highlight the distinct transcriptomic responses of different *Ae. aegypti* strains to ZIKV. This study enhances our understanding of pathogen-vector interactions and may contribute to the development of targeted strategies for ZIKV control.

CRediT authorship contribution statement

Chunling Zhu: Investigation, Methodology, Formal analysis, Data curation, Writing – review & editing. **Yuting Jiang:** Data curation, Writing – original draft, Writing – review & editing. **Qianghui Zhang:** Software, Formal analysis, Writing – review & editing. **Jian Gao:** Data curation, Writing – review & editing. **Chaojie Li:** Software, Validation, Writing – review & editing. **Chunxiao Li:** Software, Validation, Writing – review & editing. **Yande Dong:** Visualization, Investigation, Writing – review & editing. **Dan Xing:** Investigation, Writing – review & editing. **Hengduan Zhang:** Investigation, Writing – review & editing. **Teng Zhao:** Investigation, Writing – review & editing. **Xiaoxia Guo:** Investigation, Methodology, Writing – original draft, Writing – review & editing, Supervision, Visualization, Funding acquisition, Formal analysis, Data curation, Conceptualization. **Tongyan Zhao:** Investigation, Methodology, Writing – original draft, Writing – review & editing, Supervision, Visualization, Funding acquisition, Formal analysis, Data curation, Conceptualization.

Ethical approval

The animal studies were carried out in strict accordance with the recommendations in the Guide for the Care and Use of Laboratory Animals and were approved by the IACUC of the State Key Laboratory of Pathogen and Biosecurity, Beijing Institute of Microbiology and Epidemiology (permit number: IACUC-IME-2017-016).

Data availability

All data generated or analyzed during this study are included in this published article and its supplementary files; the latter are also available at https://maipdf.cn/est/a67bb028c34ee5/pdf.

Funding

This work was funded by grants from the Infective Diseases Prevention and Cure Project of China (No. 2017ZX10303404).

Declaration of competing interests

The authors declare that they have no known competing financial interests or personal relationships that could have appeared to influence the work reported in this paper.

Appendix A. Supplementary data

Supplementary data to this article can be found online at https://doi.org/10.1016/j.crpvbd.2025.100251.

References

Almeida, L.S., Nishiyama-Jr, M.Y., Pedroso, A., Costa-da-Silva, A.L., Ioshino, R.S., Capurro, M.L., Suesdek, L., 2023. Transcriptome profiling and calreticulin expression in Zika virus-infected *Aedes aegypti*. Infect. Genet. Evol. 107, 105390. https://doi.org/10.1016/j.meegid.2022.105390.

Araújo, T.V.B., Rodrigues, L.C., de Alencar Ximenes, R.A., de Barros Miranda-Filho, D., Montarroyos, U.R., et al., 2016. Association between Zika virus infection and microcephaly in Brazil, January to May, 2016: Preliminary report of a case-control study. Lancet Infect. Dis. 16, 1356–1363. https://doi.org/10.1016/S1473-3099(16)30318-8.

Audic, S., Claverie, J.M., 1997. The significance of digital gene expression profiles. Genome Res. 7, 986–995. https://doi.org/10.1101/gr.7.10.986.

Brady, O.J., Osgood-Zimmerman, A., Kassebaum, N.J., Ray, S.E., de Araujo, V.E.M., da Nobrega, A.A., et al., 2019. The association between Zika virus infection and microcephaly in Brazil 2015–2017: An observational analysis of over 4 million births. PLoS Med. 16, e1002755. https://doi.org/10.1371/journal.pmed.1002755.

Chin, C.H., Chen, S.H., Wu, H.H., Ho, C.W., Ko, M.T., Lin, C.Y., 2014. cytoHubba: Identifying hub objects and sub-networks from complex interactome. BMC Syst. Biol. 8 (Suppl. 4), S11. https://doi.org/10.1186/1752-0509-8-s4-s11.

Cock, P.J., Fields, C.J., Goto, N., Heuer, M.L., Rice, P.M., 2010. The Sanger FASTQ file format for sequences with quality scores, and the Solexa/Illumina FASTQ variants. Nucl. Acids Res. 38, 1767–1771. https://doi.org/10.1093/nar/gkp1137.

Cui, Y., Grant, D.G., Lin, J., Yu, X., Franz, A.W.E., 2019. Zika virus dissemination from the midgut of *Aedes aegypti* is facilitated by bloodmeal-mediated structural modification of the midgut basal lamina. Viruses 11, 1056. https://doi.org/10.3390/v11111056.

Deng, Y.Q., Zhao, H., Li, X.F., Zhang, N.N., Liu, Z.Y., Jiang, T., et al., 2016. Isolation, identification and genomic characterization of the Asian lineage Zika virus imported to China. Sci. China Life Sci. 59, 428–430. https://doi.org/10.1007/s11427-016-5043-4.

Dick, G.W., Kitchen, S.F., Haddow, A.J., 1952. Zika virus. I. Isolations and serological specificity. Trans. R. Soc. Trop. Med. Hyg. 46, 509–520. https://doi.org/10.1016/0035-9203(52)90042-4.

Etebari, K., Hegde, S., Saldana, M.A., Widen, S.G., Wood, T.G., Asgari, S., Hughes, G.L., 2017. Global transcriptome analysis of *Aedes aegypti* mosquitoes in response to Zika virus infection. mSphere 2. https://doi.org/10.1128/mSphere.00456-17.

Franz, A.W., Kantor, A.M., Passarelli, A.L., Clem, R.J., 2015. Tissue barriers to arbovirus infection in mosquitoes. Viruses 7, 3741–3767. https://doi.org/10.3390/v7072795.

Hussain, M., Bradshaw, T., Lee, M., Asgari, S., 2022. The involvement of atlastin in dengue virus and *Wolbachia* infection in *Aedes aegypti* and its regulation by aae-miR-989. Microbiol. Spectr. 10, e0225822. https://doi.org/10.1128/spectrum.02258-22.

Jia, N., Jiang, Y., Jian, X., Cai, T., Liu, Q., Liu, Y., et al., 2023. Transcriptome analysis of response to Zika virus infection in two *Aedes albopictus* strains with different vector competence. Int. J. Mol. Sci. 24, 4257. https://doi.org/10.3390/ijms24054257.

Kim, D., Langmead, B., Salzberg, S.L., 2015. HISAT: A fast spliced aligner with low memory requirements. Nat. Methods 12, 357–360. https://doi.org/10.1038/nmeth.3317.

Langmead, B., Salzberg, S.L., 2012. Fast gapped-read alignment with Bowtie 2. Nat. Methods 9, 357–359. https://doi.org/10.1038/nmeth.1923.

Lecona-Valera, A.N., Tao, D., Rodriguez, M.H., Lopez, T., Dinglasan, R.R., Rodriguez, M. C., 2016. An antibody against an *Anopheles albimanus* midgut myosin reduces *Plasmodium berghei* oocyst development. Parasites Vectors 9, 274. https://doi.org/10.1186/s13071-016-1548-8.

Leonhard, S.E., Bresani-Salvi, C.C., Lyra Batista, J.D., Cunha, S., Jacobs, B.C., Brito Ferreira, M.L., et al., 2020. Guillain-Barre syndrome related to Zika virus infection: A systematic review and meta-analysis of the clinical and electrophysiological phenotype. PLoS Negl. Trop. Dis. 14, e0008264. https://doi.org/10.1371/journal.pntd.0008264.

Lessler, J., Chaisson, L.H., Kucirka, L.M., Bi, Q., Grantz, K., Salje, H., et al., 2016. Assessing the global threat from Zika virus. Science 353, aaf8160. https://doi.org/10.1126/science.aaf8160.

Li, B., Dewey, C.N., 2011. RSEM: Accurate transcript quantification from RNA-Seq data with or without a reference genome. BMC Bioinf. 12, 323. https://doi.org/10.1186/1471-2105-12-323.

Licciardi, S., Loire, E., Cardinale, E., Gislard, M., Dubois, E., Cetre-Sossah, C., 2020. *In vitro* shared transcriptomic responses of *Aedes aegypti* to arboviral infections: Example of dengue and Rift Valley fever viruses. Parasites Vectors 13, 395. https://doi.org/10.1186/s13071-020-04253-5.

Livak, K.J., Schmittgen, T.D., 2001. Analysis of relative gene expression data using real-time quantitative PCR and the 2(-Delta Delta C(T)) method. Methods 25, 402–408. https://doi.org/10.1006/meth.2001.1262.

Londono-Renteria, B., Troupin, A., Conway, M.J., Vesely, D., Ledizet, M., Roundy, C.M., et al., 2015. Dengue virus infection of *Aedes aegypti* requires a putative cysteine rich venom protein. PLoS Pathog. 11, e1005202. https://doi.org/10.1371/journal.ppat.1005202.

Ma, G., Chen, L., Luo, J., Wang, B., Wang, C., Li, M., et al., 2018. Histone acetyl transferase TIP60 inhibits the replication of influenza a virus by activation the TBK1-IRF3 pathway. Virol. J. 15, 172. https://doi.org/10.1186/s12985-018-1079-3.

Macnamara, F.N., 1954. Zika virus: A report on three cases of human infection during an epidemic of jaundice in Nigeria. Trans. R. Soc. Trop. Med. Hyg. 48, 139–145. https://doi.org/10.1016/0035-9203(54)90006-1.

Prince, B.C., Walsh, E., Torres, T.Z.B., Ruckert, C., 2023. Recognition of arboviruses by the mosquito immune system. Biomolecules 13, 1159. https://doi.org/10.3390/biom13071159.

Sanchez-Vargas, I., Olson, K.E., Black, W.C., 2021. The genetic basis for salivary gland barriers to arboviral transmission. Insects 12, 73. https://doi.org/10.3390/insects12010073.

Sun, J., Zhang, W., Tan, Z., Zheng, C., Tang, Y., Ke, X., et al., 2020. Zika virus promotes CCN1 expression via the CaMKIIalpha-CREB pathway in astrocytes. Virulence 11, 113–131. https://doi.org/10.1080/21505594.2020.1715189.

Szklarczyk, D., Gable, A.L., Lyon, D., Junge, A., Wyder, S., Huerta-Cepas, J., et al., 2019. STRING v11: Protein-protein association networks with increased coverage, supporting functional discovery in genome-wide experimental datasets. Nucl. Acids Res. 47, D607–D613. https://doi.org/10.1093/nar/gky1131.

Tikhe, C.V., Cardoso-Jaime, V., Dong, S., Rutkowski, N., Dimopoulos, G., 2022. Trypsin-like inhibitor domain (TIL)-harboring protein is essential for *Aedes aegypti* reproduction. Int. J. Mol. Sci. 13, 7736. https://doi.org/10.3390/ijms23147736.

Wang, C., Wang, T., Hu, R., Duan, L., Hou, Q., Han, Y., et al., 2023. 9-butyl-harmol exerts antiviral activity against Newcastle disease virus through targeting GSK-3beta and HSP90beta. J. Virol. 97, e0198422. https://doi.org/10.1128/jvi.01984-22.

Wei, M., Zhang, Y., Aweya, J.J., Wang, F., Li, S., Lun, J., et al., 2019. *Litopenaeus vannamei* Src64B restricts white spot syndrome virus replication by modulating apoptosis. Fish Shellfish Immunol. 93, 313–321. https://doi.org/10.1016/j.fsi.2019.07.062.

WHO, 2022. Zika virus. World Health Organization, Geneva, Switzerland. https://www.who.int/news-room/fact-sheets/detail/zika-virus.

Zhu, C., Jiang, Y., Zhang, Q., Gao, J., Li, C., Li, C., Dong, Y., et al., 2021. Vector competence of *Aedes aegypti* and screening for differentially expressed microRNAs exposed to Zika virus. Parasites Vectors 14, 504. https://doi.org/10.1186/s13071-021-05007-7.

Zimler, R.A., Yee, D.A., Alto, B.W., 2021. Transmission potential of Zika virus by *Aedes aegypti* (Diptera: Culicidae) and *Ae. mediovittatus* (Diptera: Culicidae) populations from Puerto Rico. J. Med. Entomol. 58, 1405–1411. https://doi.org/10.1093/jme/tjaa286.